Applied Catalysis A: General 378 (2010) 227–233

Contents lists available at ScienceDirect

Applied Catalysis A: General

journal homepage: www.elsevier.com/locate/apcata

Light-induced photocatalytic degradation of stearic acid by *c*-axis oriented ZnO nanowires

G. Kenanakis [a,b,c,d,*], N. Katsarakis [a,c,d]

[a] Center of Materials Technology and Laser, School of Applied Technology, Technological Educational Institute of Crete, 710 04 Heraklion, Crete, Greece
[b] Department of Chemistry, University of Crete, 710 03 Heraklion, Crete, Greece
[c] Institute of Electronic Structure and Laser, Foundation for Research & Technology-Hellas, P.O. Box 1527, Vassilika Vouton, 711 10 Heraklion, Crete, Greece
[d] Science Department, School of Applied Technology, Technological Educational Institute of Crete, 710 04 Heraklion, Crete, Greece

ARTICLE INFO

Article history:
Received 13 January 2010
Received in revised form 19 February 2010
Accepted 22 February 2010
Available online 1 March 2010

Keywords:
Nanowires
Photocatalysis
Aqueous solution growth
Seed layer
ZnO
Stearic acid

ABSTRACT

The photocatalytic activity of highly *c*-axis oriented ZnO nanowires' arrays grown on seeded glass substrates from aqueous solutions was investigated against the degradation of stearic acid under UV-A light illumination (365 nm). All chemically grown ZnO samples show very good crystallinity and high transmittance in the visible region. The nanowires' diameter ranges from 35 ± 5 nm to 160 ± 10 nm depending on the grain size of the seed layer applied, while their length (1–1.2 μm) is mainly affected from growth time. It is demonstrated that ZnO nanowires' arrays show superior photocatalytic activity compared with the stand-alone seed layers, probably due to their enhanced crystallinity and larger surface-to-volume ratio.

1. Introduction

Environmental contamination is a growing problem that cannot be neglected as it influences our world and daily life. A solution for this issue can be found in the field of semiconductor chemistry, in particular heterogeneous photocatalysis, which implies the use of an inert catalyst, non-hazardous oxidants and UV and/or visible light input. Heterogeneous photocatalysis is attracting extensive interest for the degradation of organic pollutants [1–6] and the production of self-cleaning [7,8] or anti-bacterial surfaces [9]. The ability of semiconductor photocatalysts, in particular TiO_2 and ZnO, to degrade a range of organic pollutants, offers many potential applications in areas, such as water and air purification and self-cleaning surfaces [1].

Among the mentioned oxide materials, ZnO is easier to grow either in the form of powder [10] or on top of various substrates [11–16] using chemical techniques, which are environmental friendly and quite easy to handle. Besides, it has been reported that ZnO shows better activity than TiO_2 in the photodegradation of some dyes in aqueous solutions since it can absorb more light quanta [17].

Up to now, many photocatalytic materials including TiO_2 and ZnO have been prepared as thin films as well as fine powders [18]. Great attention has been given to fine powders since high photocatalytic efficiency can be achieved by increasing the effective surface area of the materials. However, these powders have mostly been used in water suspensions, which limits their practical use due to difficulties in their separation and recovery. Supporting photocatalytic materials on a steady substrate can eliminate this issue. Many thin film deposition techniques have been widely used for the immobilization of photocatalytic materials [19,20].

The activity of photocatalytic ZnO films can vary considerably and is dependent on many factors, such as film thickness, roughness, grain size and deposition temperature, to name but a few. Meanwhile, since photocatalytic activity increases with effective surface area, a rough film surface with a high surface-to-volume ratio is beneficial. On the other hand, one-dimensional nanostructured samples offer enhanced photocatalytic efficiency due to their extremely high surface-to-volume ratio [21,22]. Thus, the successful exploitation of nanostructured ZnO thin films for use in photocatalytic applications requires the development of techniques for controlling their morphology and structural properties.

In this work, we investigate the photocatalytic activity of ZnO nanowires' arrays grown on glass substrates from aqueous solu-

* Corresponding author at: Institute of Electronic Structure and Laser (IESL), Foundation for Research & Technology-Hellas (FORTH), P.O. Box 1385, Vassilika Vouton, 711 10 Heraklion, Greece. Tel.: +30 2810391917; fax: +30 2810391305.
E-mail address: gkenanak@iesl.forth.gr (G. Kenanakis).

0926-860X/$ – see front matter © 2010 Elsevier B.V. All rights reserved.
doi:10.1016/j.apcata.2010.02.030

tion according to the approach of Andrés Vergés et al. [11] and Vayssieres [12]. It is demonstrated that seeded glass substrates are necessary in order to produce highly *c*-axis oriented ZnO nanowires [23], whose diameter can be accurately tuned by varying the grain size of the seed layer. On the other hand, the nanowires' length is mainly determined by growth time. The influence of nanowires' crystallinity, morphology and dimensions on their photocatalytic activity against the degradation of stearic acid is studied. We provide evidence that ZnO nanowires' arrays show enhanced photocatalytic activity compared to the as-deposited seed layers, which can be mostly attributed to their good crystallinity and enhanced surface-to-volume ratio.

2. Experimental details

2.1. Deposition of ZnO seed layers and nanowires

ZnO thin films with a thickness of 30–210 nm, which were subsequently used as seed layers for the aqueous solution growth of ZnO nanowires' arrays, were deposited on glass (Corning Inc. 7059) substrates using the sol–gel/spin-coating technique reported elsewhere [23,24]. In brief, zinc acetate dehydrate [$Zn(CH_3COO)_2{\cdot}2H_2O$] was first dissolved in a mixture of 2-methoxy ethanol and monoethanolamine at room temperature (RT). The concentration of zinc acetate was 0.75 mol/L and the molar ratio of monoethanolamine to zinc acetate was kept at 1:1. The resultant solution was stirred for 1 h at 60 °C to yield a homogeneous, clear and transparent solution using a magnetic stirrer. The deposition was usually performed within 24 h after the solution was prepared, by spin-coating the substrates, which were rotated at 3000 rpm for 20 s. After processing, the substrates were preheated at 350 °C for 10 min to evaporate the solvent and remove the organic residuals in the films. This procedure was repeated up to 10 times. The films were then annealed in air at 600 °C for 60 min. The thickness of the films was measured using a stylus profilometer (alpha-step 100, Tencor).

ZnO nanowires' arrays were subsequently grown on Corning glass substrates, pre-coated with 1×–10× ZnO seed layers deposited via the sol–gel technique, using an equimolar (0.01 M) aqueous solution of $Zn(NO_3)_2{\cdot}6H_2O$ and $C_6H_{12}N_4$ [11,12,25]. Firstly, laboratory Pyrex glass bottles with polypropylene autoclavable screw caps were filled with the solution described above. Subsequently, the substrates pre-coated with the ZnO seed layers were placed in the bottles facing downwards and heated at a constant temperature of 95 °C for 5 h in a regular laboratory oven. The samples were then thoroughly washed with MilliQ (18.2 MΩ cm) water to eliminate residual salts or amino complexes, and dried in air at the same temperature. Prior to deposition, all substrates used were cleaned using a Piranha solution (H_2SO_4/H_2O_2 = 3/1), rinsed with MilliQ water and dried under N_2 gas flow.

2.2. Characterization techniques

The crystal structure of the ZnO samples was determined by X-ray diffraction (XRD) using a Rigaku (RINT 2000) diffractometer with Cu *Kα* X-rays, while their surface morphology was studied by means of a field emission scanning electron microscope (FE-SEM, JEOL JSM-7000F) and an atomic force microscope (AFM) in tapping mode (Digital Instruments – Nanoscope IIIa). The surface roughness (RMS) of the ZnO seed layers was determined using the scanning probe image processor (SPIP, v. 3.3.5.0) image processing software for nano- and micro-scale microscopy from Image Metrology. Finally, UV–vis transmission spectra were recorded using a Shimadzu UV-2401 spectrophotometer over the wavelength range of 190–990 nm.

2.3. Photocatalytic activity study

There are many different methods that can be used to determine the activity of photocatalytic surfaces. Popular techniques include those based on the photo-oxidation of organic films such as stearic acid (SA) [19,26–30] or organic vapours [31] and contact angle changes [32].

The photocatalytic activity of our ZnO samples was determined using stearic acid as a model compound, in which a thin layer of SA is deposited onto the film and its photocatalytic destruction is monitored as a function of time [26–30]. This method has gained preference over the years since SA provides a reasonable model compound for solid films that deposit on exterior and interior surfaces. Moreover, SA is very stable under UV illumination in the absence of a photocatalyst film (phenomenon of photolysis). Furthermore, SA can be easily laid down from a methanol or chloroform solution making the test much easier.

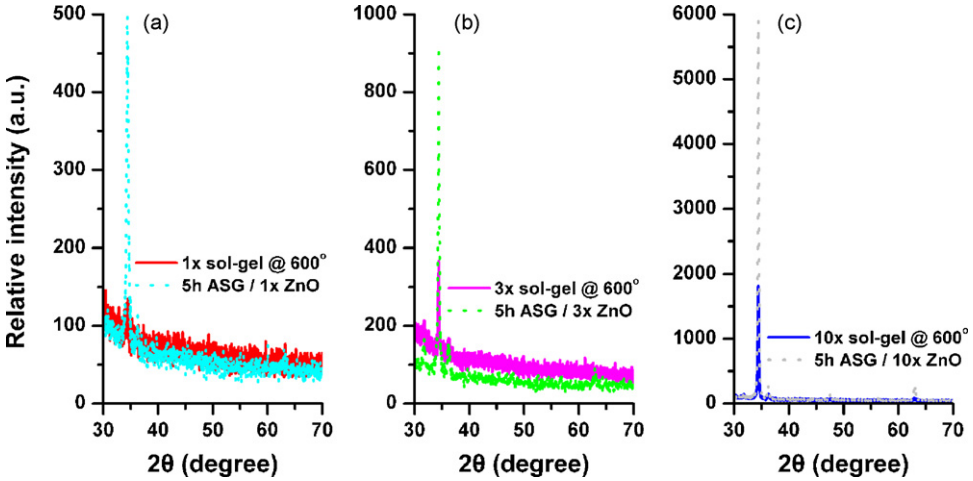

Fig. 1. XRD patterns of (a) ZnO nanowires grown by aqueous solution growth (ASG) for 5 h (cyan dotted curve) on Corning glass substrates pre-coated with a 30 nm-thick ZnO seed layer (red solid curve), (b) ZnO nanowires grown by ASG for 5 h (green dotted curve) on Corning glass substrates pre-coated with a 75 nm-thick ZnO seed layer (magenta solid curve), and (c) ZnO nanowires grown by ASG for 5 h (blue dotted curve) on Corning glass substrates pre-coated with a 210 nm-thick ZnO seed layer (red solid curve). (For interpretation of the references to color in this figure legend, the reader is referred to the web version of this article.)

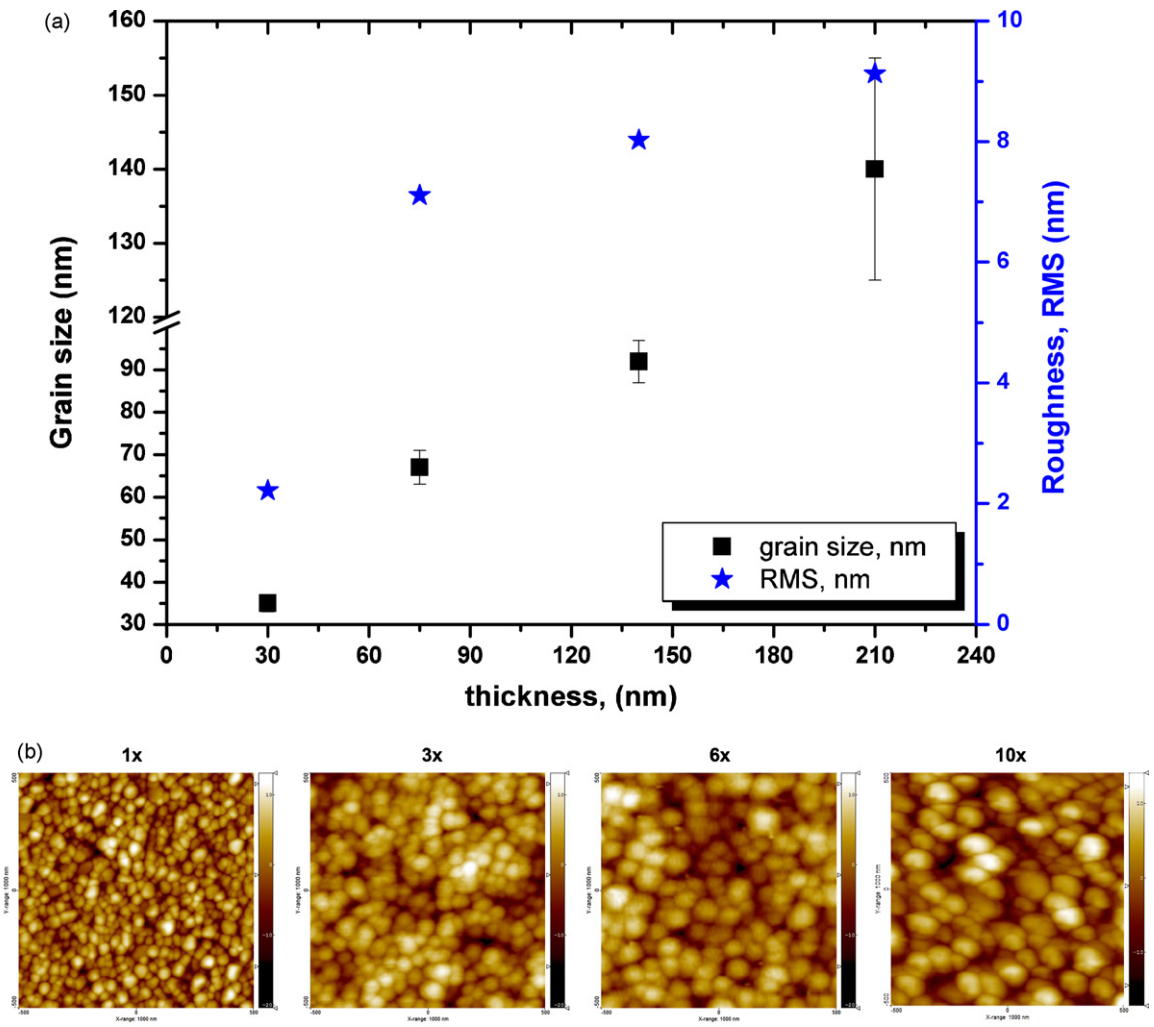

Fig. 2. (a) Grain size (black squares) and roughness (blue stars) vs. thickness of the sol–gel deposited ZnO seed layers on Corning glass annealed at 600 °C and (b) AFM images (scan size 1 μm × 1 μm) of (left to right) 30 nm- (1×), 75 nm- (3×), 140 nm- (6×) and 210 nm-thick (10×) ZnO seed layers on Corning substrates. (For interpretation of the references to color in this figure legend, the reader is referred to the web version of this article.)

In order to deposit stearic acid on the ZnO films and nanostructures, a droplet of 30 μL of a 0.1 M stearic acid solution in chloroform was spin-coated on the sample surface under test at a rotation speed of 500 rpm for 30 s. Samples were then dried at 80° C in air for 10 min.

The decomposition of stearic acid can be demonstrated by FT-IR spectroscopy through the monitoring of the asymmetric C–H stretching mode of the CH_3 group at 2958 cm^{-1} and the asymmetric and symmetric C–H stretching modes of the CH_2 group at 2923 cm^{-1} and 2853 cm^{-1}, respectively. The photocatalytic activity experiments on all ZnO samples for the decomposition of stearic acid were performed at ambient temperature. The integrated area of the stearic acid C–H stretching peaks (2800–3000 cm^{-1}) was monitored using a Fourier transform infrared spectrometer (FT-IR, IRPrestige-21, Shimadzu) before and after black light illumination in a box reactor at certain time intervals. The light source used was an HPK 125 W Philips mercury lamp with main emission wavelength at 365 nm and an incident light intensity of 10 mW/cm^2. For ease in comparison of the photocatalytic activity between different samples, the integrated area of the C–H stretching peaks (2800–3000 cm^{-1}) measured at each irradiation time interval was normalized to the initial integrated area (prior to the irradiation) in order to calculate the percentage of stearic acid remaining as a function of irradiation time.

3. Results and discussion

Fig. 1 depicts X-ray diffraction patterns of ZnO seed layers deposited by the sol–gel/spin-coating technique and nanowires' arrays grown by aqueous solution growth on Corning glass substrates pre-coated with 1, 3 or 10 ZnO seed layers (Fig. 1a–c). The thickness of the seed layers applied is 30 nm, 75 nm and 210 nm for the 1×, 3× and 10× ZnO samples, respectively. All the diffraction peaks observed are in good agreement with the JCPDS card (No. 36-1451) for a typical hexagonal wurtzite type ZnO crystal. It can be also seen that no other characteristic peaks corresponding to possible impurities, such as zinc nitrate or zinc hydroxide, are observed in the XRD patterns.

Red solid line in Fig. 1a depicts the X-ray diffraction pattern of a 30 nm-thick ZnO seed layer deposited by sol–gel at 600 °C on Corning glass. There is no evidence of any diffraction peaks, indicating that the film was largely amorphous. On the other hand, ZnO samples prepared via aqueous solution growth for 5 h on Corning glass substrates pre-coated with a 30 nm-thick ZnO seed layer show a clear preferential growth orientation along the (0 0 2) crystallographic direction, i.e., perpendicular to the Corning glass substrates (cyan dotted line, Fig. 1a). The reason for superior alignment on ZnO seeded substrates is due to the polar nature of the ZnO surface and the matching lattice structure [33].

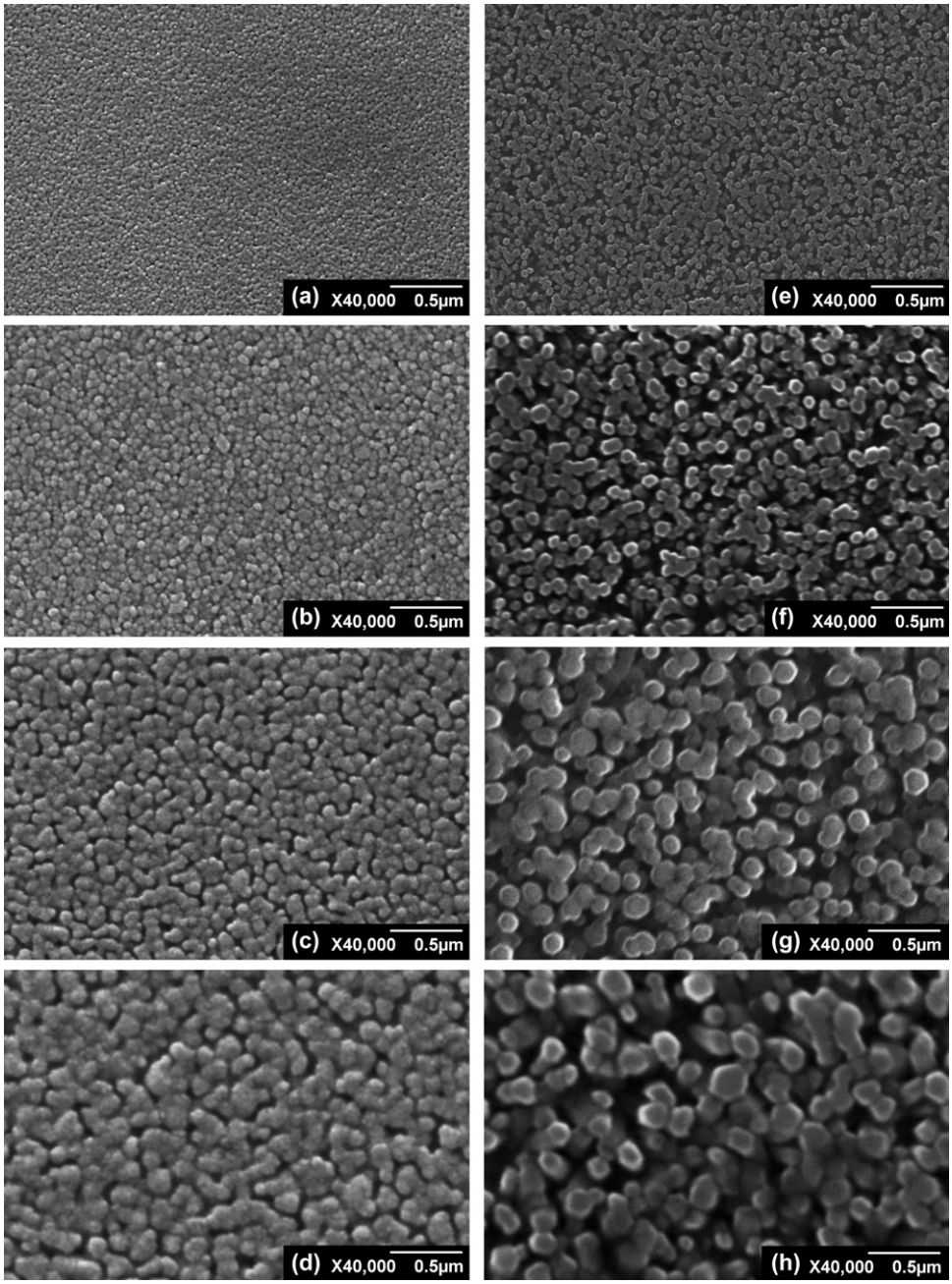

Fig. 3. SEM images of (a–d) 30 nm-, 75 nm-, 140 nm- and 210 nm-thick ZnO seed layers, respectively, grown by sol–gel technique and (e–h) ZnO nanowires deposited by aqueous solution growth for 5 h on Corning glass substrates pre-coated with 30 nm-, 75 nm-, 140 nm- and 210 nm-thick seed layers, respectively.

Fig. 1b and c displays the X-ray diffraction patterns of 75 nm- and 210 nm-thick ZnO seed layers deposited on Corning glass substrates by sol–gel at 600 °C (magenta and blue solid lines in Fig. 1b and c, respectively), along with those of the ZnO samples grown via aqueous solution growth for 5 h on top of Corning glass substrates pre-coated with 75 nm- and 210 nm-thick ZnO seed layers (green and grey dotted lines in Fig. 1b and c, respectively). Once more, it can be readily observed that only the (0 0 2) diffraction peak occurs, demonstrating that there is a preferred growth orientation along the *c*-axis, i.e., perpendicular to the substrate used. This preferential growth orientation is directly related to the presence of the ZnO seed layers [34].

As it can be observed in Fig. 1b and c, both the 3× and 10× seed layers exhibit the ZnO wurtzite hexagonal structure and grow preferentially along the (0 0 2) direction. Therefore, they indeed act as seed layers and assist the preferential growth of the chemically grown ZnO samples along the *c*-axis, i.e., the (0 0 2) crystallographic direction. Moreover, it can be observed that the samples deposited by aqueous solution growth show narrower (0 0 2) reflections with significantly higher intensity than the corresponding seed layers (Fig. 1a–c). The Full Width at Half Maximum (FWHM) value for the (0 0 2) peak varies between 0.203° and 0.243° for the 75 nm- and 210 nm-thick ZnO seed layers, while it is in the range of 0.175–0.215° for the ZnO samples grown via aqueous solution growth for 5 h on the glass substrates pre-coated with the 75 nm- and 210 nm-thick ZnO seed layers, respectively. It is therefore concluded that the occurrence of a thin ZnO seed layer is crucial for the growth of well-crystalline (0 0 2) oriented ZnO samples onto Corning glass substrates.

Fig. 2a exhibits the variation of grain size and surface roughness (RMS) of the as-grown ZnO seed layers as a function of thickness. The grain size as well as the roughness gradually increases with

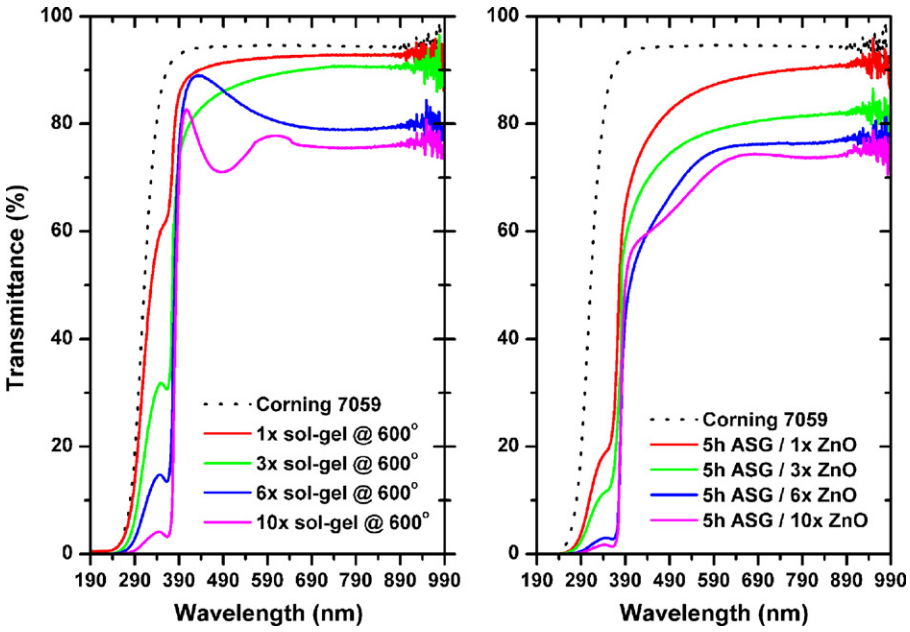

Fig. 4. Optical transmittance spectra of (a) 30 nm- (1×), 75 nm- (3×), 140 nm- (6×) and 210 nm-thick (10×) ZnO seed layers, respectively, grown by sol–gel technique and (b) ZnO nanowires deposited by aqueous solution growth for 5 h on Corning glass substrates pre-coated with 30 nm- (1×), 75 nm- (3×), 140 nm- (6×) and 210 nm-thick (10×) seed layers, respectively.

thickness, i.e., the number of the spin-coated layers (see Fig. 2b). In particular, the 1× ZnO seed layer with a thickness of around 30 nm has a grain size of ~35 ± 2 nm and a roughness of ~2 nm, while the 3× ZnO seed layer with a thickness of ~75 nm, has a grain size of ~67 ± 4 nm and a roughness of ~7 nm. These grain size and roughness values become even higher for the cases of the 6× ZnO seed layer (thickness ~140 nm, grain size ~92 ± 5 nm, and roughness ~8 nm) and the 10× ZnO seed layer (thickness ~210 nm, grain size ~140 ± 15 nm, and roughness ~9 nm).

Fig. 3a–d presents SEM micrographs of the 30 nm-, 75 nm-, 140 nm- and 210 nm-thick ZnO seed layers, i.e., 1×, 3×, 6× and 10× spin-coated layers, respectively, deposited by the sol–gel technique at 600 °C on Corning glass substrates. It can be observed that the layers are homogeneous, crack-free and densely packed, while their grains become more uniform and bigger in size as the thickness increases. As it is shown in Figs. 2 and 3a–d there is a good agreement between the results revealed from AFM and SEM analysis regarding the grain size and the surface morphology of the ZnO seed layers.

Fig. 3e–h illustrates SEM images of the ZnO samples deposited by aqueous solution growth for 5 h on Corning glass substrates pre-coated with 30 nm-, 75 nm-, 140 nm- and 210 nm-thick ZnO seed layers (Fig. 3a–d), respectively. As it can be observed, in all cases, the substrates were covered with quite dense and uniform ZnO nanowire arrays. These nanowires emerge perpendicular to the substrate applied, with almost no nanowires tilted from the surface, while they all display a hexagonal cross-section. These remarks are in agreement with the XRD results, which clearly demonstrate that the ZnO samples deposited by aqueous solution growth on seeded Corning glass substrates exhibit the wurtzite hexagonal crystal structure and show a preferential growth orientation along the (0 0 2) direction (see Fig. 1). It is furthermore observed that the nanowires' diameter increases with the seed layer thickness. As the seed layer thickness increases from 30 nm to 210 nm, the wires' diameter rises from ~35 ± 5 nm to ~160 ± 10 nm. This increase in the wires' diameter is directly related to the grain size of the ZnO seed layer. The grain size gradually increases with thickness, i.e., the number of the spin-coated layers (see Fig. 2). As it can be seen from Fig. 3e, the diameter of the ZnO nanowires grown on a 30 nm-thick seed layer (see Fig. 3a) is ~35 ± 5 nm, almost equal to the grain size of the 1× ZnO seed layer, i.e., ~35 ± 2 nm (see Figs. 2 and 3a). The diameter of the ZnO nanowires grown on 75 nm-, 140 nm- and 210 nm-thick seed layers is ~65 ± 5 nm, ~105 ± 15 nm and ~160 ± 10 nm, respectively (see Fig. 3f–h), quite close to the grain size values of the corresponding ZnO seed layers (see Figs. 2 and 3b–d). It is therefore concluded that the occurrence of a ZnO seed layer is not only indispensable for obtaining well-oriented ZnO nanowires onto Corning glass substrates via aqueous solution growth, but its grain size controls accurately the ZnO nanowires' diameter.

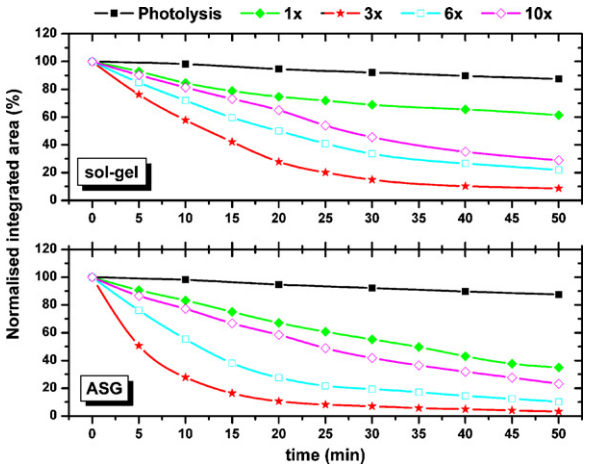

Fig. 5. Normalized integrated area vs. irradiation time for (top) 30 nm- (1×, green solid rhombuses), 75 nm- (3×, red stars), 140 nm- (6×, cyan open squares) and 210 nm-thick (10×, magenta open rhombuses) ZnO seed layers, respectively grown by sol–gel technique and (bottom) ZnO nanowires deposited by aqueous solution growth for 5 h on Corning glass substrates pre-coated with 30 nm- (1×, green solid rhombuses), 75 nm- (3×, red stars), 140 nm- (6×, cyan open squares) and 210 nm-thick (10×, magenta open rhombuses) seed layers, respectively. For comparison reasons, the photolysis curve (black solid squares) is also presented. (For interpretation of the references to color in this figure legend, the reader is referred to the web version of this article.)

Table 1
Photocatalytic activity of ZnO seed layers and nanowires regarding the degradation of stearic acid at 30 min.

	Photolysis	1×	ASG/1×	3×	ASG/3×	6×	ASG/6×	10×	ASG/10×
α (%) at 30 min	7.85	31.11	44.85	85.08	93.02	66.43	80.59	54.45	58.21

For every case of Fig. 3f–h, i.e., 5 h aqueous solution growth on 75 nm-, 140 nm- and 210 nm-thick ZnO seed layers respectively, the length of the as-grown ZnO nanowires is in the range of 1–1.2 μm, indicating that the only parameter that affects the nanowires' length is growth time [35]. The length of the ZnO nanowires grown on a 30 nm-thick seed layer is quite smaller, ~400–500 nm, probably due to the poor crystallinity of the corresponding 1× ZnO seed layer (see Fig. 1a) and is currently under further investigation.

Taking into consideration the nanowires' dimensions mentioned above, i.e., their diameter and length, we can estimate the aspect ratio (length over diameter, L/D) of the ZnO nanowires grown on Corning glass substrates pre-coated with 30 nm-, 75 nm-, 140 nm- and 210 nm-thick seed layers. (L/D) is a commonly used parameter which indicates the surface-to-volume ratio of nanostructured samples. ZnO nanowires grown on a 30 nm-thick seed layer have an aspect ratio (L/D) of ~12.5, while L/D becomes ~17.2, ~12 and ~8 for the cases of 5 h aqueous solution growth on 75 nm-, 140 nm- and 210 nm-thick seed layers, respectively. Thus, we could state that the aspect ratio becomes higher, i.e., ~17.2, for the case of 5 h aqueous solution growth on a 75 nm-thick ZnO seed layer which, as already mentioned, is the polycrystalline seed layer with the smaller grain size, i.e., ~67 ± 4 nm (see Figs. 1b, 2 and 3b).

The optical transmittance spectra of the ZnO seed layers and the nanowires' arrays in the wavelength region 190–990 nm are presented in Fig. 4. All the samples are highly transparent in the visible regime and exhibit a sharp absorption band in the UV region. A clear excitonic nature of the transmittance spectra is visible for both ZnO seed layers and nanowires. The presence of this excitonic peak at ~350 nm is attributed to a minimum strain and improved crystalline quality with increase in thickness [36]. It can be noted that increasing the ZnO seed layers' thickness from 30 nm to 210 nm leads to a decrease in transmittance from 92% to 78% at 600 nm, while the corresponding drop in the transmittance for the case of 5 h aqueous solution growth on 30 nm- and 210 nm-thick seed layers ranges from 88% to 72%, respectively. This reduction in the transmittance can be attributed to the increase of the samples' thickness. It is quite interesting that the chemically grown ZnO nanowires display similar transmittance values with those observed for the ZnO seed layers alone. For example, ZnO nanowires grown for 5 h on a 75 nm-thick ZnO seed layer exhibit 89% transmittance at 600 nm, while a 75 nm-thick ZnO seed layer shows 79% transmittance at the same wavelength (see Fig. 4).

Fig. 5 presents the normalized integrated area vs. irradiation time curves for both ZnO seed layers deposited by the sol–gel technique (see top side of Fig. 5) and nanowires fabricated by aqueous solution growth (see Fig. 5, bottom). It can be noticed that all ZnO samples show remarkable photocatalytic activity, degrading stearic acid by more than 40% at 50 min. This is most probably due to their good crystallinity and large effective surface area. In particular, ZnO nanowires grown on seeded Corning glass substrates are more efficient in terms of photocatalysis than the stand-alone seed layers, probably due to their higher surface-to-volume ratio. For example, ZnO nanowires synthesized via aqueous solution growth for 5 h on a 75 nm-thick seed layer show outstanding photocatalytic activity, degrading stearic acid by ~93.02% at 30 min (see red line with solid stars in Fig. 5, bottom), while the corresponding seed layer itself shows an activity of ~85.08% (see red line with solid stars in Fig. 5, up). For comparison reasons, the photolysis curve (no catalyst present) is also displayed in Fig. 5 (black solid squares). It can be seen that the UV light results only in ~7.85% and ~12.45% degradation of stearic acid after 30 min and 50 min of exposure, respectively.

The photocatalytic activity of the ZnO seed layers and nanowires' arrays at 30 min is summarized in Table 1. It can be observed that among ZnO seed layers, the 75 nm-thick one (3×) shows better activity (85.08%) since, as already mentioned, this is the polycrystalline seed layer with the smaller grain size, i.e., ~67 ± 4 nm (see Figs. 1b, 2 and 3b) and thus higher surface area. The 210 nm-thick seed layer is less efficient than the 75 nm-thick one, showing a photocatalytic activity of ~66.43% at 30 min, since its grain size is much bigger, in the range of ~140 ± 15 nm, giving a smaller surface area. Finally, as expected, the 30 nm-thick seed layer exhibits the least photocatalytic activity (31.11%) due to its poor crystallinity (see Fig. 1a).

As presented in Table 1, ZnO nanowires grown on a 30 nm-thick seed layer, with an aspect ratio (L/D) of ~12.5, show a photocatalytic activity of ~44.85%, while as (L/D) increases the photocatalytic activity rises, reaching ~93.02% for the case of 5 h aqueous solution growth on a 75 nm-thick seed layer (aspect ratio (L/D) ~17.2). As the seed layer's thickness further increases to 140 nm and 210 nm, the aspect ratio of the as-grown ZnO nanowires decreases to ~12 and ~8, respectively. The decrease of (L/D) results in a reduction of the ZnO nanowires' photocatalytic activity at 30 min to 80.59% and 58.21% for samples grown on Corning glass substrates pre-coated with 140 nm- and 210 nm-thick ZnO seed layers, respectively. Higher aspect ratio (L/D) values correspond to an increase of the surface-to-volume ratio, which in advance leads to an enhancement of the photocatalytic activity [21–22]. Finally, it can be concluded that high aspect ratios of the nanowires formed, along with enhanced crystallinity result in significant photocatalytic activity.

4. Conclusions

ZnO nanowires, highly oriented along *c*-axis, were grown from an aqueous solution on Corning glass substrates pre-coated with 30 nm- up to 210 nm-thick ZnO seed layers deposited via the sol–gel technique. All chemically grown ZnO samples show very good crystallinity and high transmittance in the visible region, while the nanowires' diameter can be accurately tuned by varying the grain size of the seed layer used. On the other hand, the nanowires' length mainly depends on growth time. All ZnO samples show remarkable photocatalytic activity regarding the degradation of stearic acid. Amongst ZnO seed layers, the 75 nm-thick one (3×) shows better photocatalytic activity, degrading stearic acid by 85.08% at 30 min, due to its good crystallinity and smaller grain size. ZnO nanowires' arrays demonstrate, however, superior photocatalytic activity compared with the stand-alone seed layers, probably because of their enhanced crystallinity and larger surface-to-volume ratio. In particular, ZnO nanowires grown for 5 h on a 75 nm-thick seed layer exhibit an outstanding photocatalytic activity, degrading stearic acid by ~93.02% at 30 min, a behaviour which is attributed to their higher aspect ratio [(L/D) ~17.2], i.e., larger surface-to-volume ratio. It is concluded that the most critical parameter affecting photocatalytic activity of the nanowires' arrays is their surface-to-volume ratio, which can be adjusted by varying the seed layer's grain size and the growth time.

References

[1] A. Mills, S. Lee, J. Photochem. Photobiol. A 152 (2002) 233–247.
[2] I.M. Arabatzis, S. Antonaraki, T. Stergiopoulos, A. Hiskia, E. Papaconstantinou, M.C. Bernard, P. Falaras, J. Photochem. Photobiol. A 149 (2002) 23–245.
[3] S.B. Kim, S.C. Hong, Appl. Catal. B: Environ. 35 (2002) 305–315.
[4] Y.H. Hsien, C.F. Chang, Y.H. Chen, S.F. Chang, Appl. Catal. B: Environ. 31 (2001) 241–249.
[5] M. Rosana, W. Alberici, F. Jardim, Appl. Catal. B: Environ. 14 (1997) 55–68.
[6] L. Xiao-e, A.N.M. Green, S.A. Haque, A. Mills, J.R. Durrant, J. Photochem. Photobiol. A 162 (2004) 253–259.
[7] K. Guan, Surf. Coat. Technol. 191 (2005) 155–160.
[8] G. Kenanakis, E. Stratakis, K. Vlachou, D. Vernardou, E. Koudoumas, N. Katsarakis, Appl. Surf. Sci. 254 (2008) 5695–5699.
[9] S.H. Lee, S. Pumprueg, B. Moudgil, W. Sigmund, Colloids Surf. B 40 (2005) 93–98.
[10] K.M. Parida, S.S. Dash, D.P. Das, J. Colloid Interface Sci. 298 (2006) 787–793.
[11] M. Andrés Vergés, M. Martinez, E. Matijević, J. Mater. Res. 8 (1993) 2916–2920.
[12] L. Vayssieres, Adv. Mater. 15 (2003) 464–466.
[13] Z. Zhang, H. Yu, Y. Wang, M.Y. Han, Nanotechnology 17 (2006) 2994–2997.
[14] J. Chen, C. Li, J.L. Song, X.W. Sun, W. Lei, W.Q. Deng, Appl. Surf. Sci. 255 (2009) 7508–7511.
[15] X. Hu, Y. Masuda, T. Ohji, K. Kato, J. Am. Ceram. Soc. 92 (4) (2009) 922–926.
[16] J.L. Yang, S.J. An, W.I. Park, G.C. Yi, W. Choi, Adv. Mater. 14 (16) (2004) 1661–1664.
[17] S. Sakthivel, B. Neppolian, M.V. Shankar, B. Arabindoo, M. Palanichamy, V. Murugesan, Sol. Energy Mater. Sol. Cells 77 (2003) 65–82.
[18] A. Mills, S. Le Hunte, J. Photochem. Photobiol. A 108 (1997) 1–35.
[19] M. Suzuki, T. Ito, Y. Taga, Appl. Phys. Lett. 78 (2001) 3968–3970.
[20] P.V. Kamat, R. Huehn, R. Nicolaescu, J. Phys. Chem. B 106 (2002) 788–794.
[21] R. Hong, T. Pan, J. Qian, H. Li, Chem. Eng. J. 119 (2006) 71–81.
[22] L. Jing, Z. Xu, X. Sun, J. Shang, W. Cai, Appl. Surf. Sci. 180 (2001) 308–314.
[23] G. Kenanakis, D. Vernardou, E. Koudoumas, N. Katsarakis, J. Cryst. Growth (2009) 4799–4804.
[24] H. Li, J. Wang, H. Liu, H. Zhang, X. Li, J. Cryst. Growth 275 (2005) 943–946.
[25] G. Kenanakis, D. Vernardou, E. Koudoumas, G. Kiriakidis, N. Katsarakis, Sens. Actuators B: Chem. 124 (2007) 187–191.
[26] A. Mills, S. Lee, A. Lepre, I.P. Parkin, S.A. O'Neill, Photochem. Photobiol. Sci. 1 (11) (2002) 865–868.
[27] A. Mills, J. Wang, Photochem. Photobiol. A 182 (2006) 181–186.
[28] T. Sawunyama, L. Jiang, A. Fujishima, K. Hashimoto, J. Phys. Chem. B 101 (1997) 11000–11003.
[29] M.E. Simonsen, H. Jensen, Z. Li, E.G. Søgaard, Photochem. Photobiol. A 200 (2008) 192–200.
[30] D. Vernardou, G. Kalogerakis, E. Stratakis, G. Kenanakis, E. Koudoumas, N. Katsarakis, Solid State Sci. 11 (2009) 1499–1502.
[31] J. Shang, W. Li, Y. Zhu, J. Mol. Catal. A: Chem. 202 (2003) 187–195.
[32] A. Mills, N. Elliott, I.P. Parkin, S.A. O'Neill, R.J. Clark, J. Photochem. Photobiol. A: Chem. 151 (2002) 171–179.
[33] Z.L. Wang, Mater. Today 7 (2004) 26–33.
[34] Q. Li, V. Kumar, Y. Li, H. Zhang, T.J. Marks, R.P.H. Chang, Chem. Mater. 17 (2005) 1001–1006.
[35] L.E. Greene, M. Law, D.H. Tan, M. Montano, J. Goldberger, G. Somorjai, P. Yang, Nano Lett. 5 (7) (2005) 1231–1236.
[36] S. Mridha, D. Basak, Mater. Res. Bull. 42 (2007) 875–882.